Experimental study of the effect of ullage height on flame characteristics of pool fires

Liu, Chunxiang; Ding, Long; Jangi, Mehdi; Ji, Jie; Yu, Longxing; Wan, Huaxian

DOI:
10.1016/j.combustflame.2020.03.009

Document Version
Peer reviewed version

Citation for published version (Harvard):
Liu, C, Ding, L, Jangi, M, Ji, J, Yu, L & Wan, H 2020, 'Experimental study of the effect of ullage height on flame characteristics of pool fires', *Combustion and Flame*, vol. 216, pp. 245-255. https://doi.org/10.1016/j.combustflame.2020.03.009

Experimental study of the effect of ullage height on flame characteristics of pool fires

Chunxiang Liu [a], Long Ding [a], Mehdi Jangi [b], Jie Ji [a, c,*], Longxing Yu [a], Huaxian Wan [a]

[a] *State Key Laboratory of Fire Science, University of Science and Technology of China, Jinzhai Road 96, Hefei, Anhui 230026, China*

[b] *School of Mechanical Engineering, University of Birmingham, Edgbaston, Birmingham B15 2TT, UK*

[c] *Institute of Advanced Technology, University of Science and Technology of China, Hefei, Anhui 230088, China*

Corresponding Author: Jie Ji (jijie232@ustc.edu.cn)

Abstract: A series of experiments were carried out to investigate the effect of ullage height, i.e. the distance between fuel surface and the pool upper rim, on flame characteristics of heptane and ethanol pool fires. The pool diameters included 10 cm, 15 cm, and 20 cm. For each pool, ullage height was increased from zero to the value that the flame self-extinguished. During each test, the ullage height was kept constant by a fuel level maintaining device. Results show that ullage height has a significant effect on flame characteristics. When the ullage height equals zero, there is a stable conical structure near the pool upper rim, above which the unstable plume develops. Under lower ullage height conditions, plume puffing happens. The unstable plume begins to initiate around the pool upper rim, then rolling and expanding upward. At the same time, its beneath flame is stretched thinner and thinner and eventually breaks from the bulk. When the ullage height further increases, plume puffing becomes less evident. While for the mass loss rate, it generally decreases with the increase of h/D. It was proved in literature that the previous flame height model is inapplicable to pool fires with large ullage height. In this paper, to consider the effect of ullage height on plume flow structures, an equivalent hydraulic diameter, $D_{eq.}$, is proposed to establish one new flame height correlation. By comparing previous model predictions with the current experimental data, it is found that conventional flame oscillation models are unsuitable to pool fires with large ullage height. Based on $D_{eq.}$, two new dimensional and dimensionless flame oscillation models were proposed according to the current experimental data. The correlated flame height model and proposed flame oscillation models were validated and agreed well with reference data.

Keywords: ullage height, flame characteristics, mass loss rate, equivalent hydraulic diameter, flame height, flame oscillation frequency

1. Introduction

Fire accident is a phenomenon of uncontrolled combustion in both time and space [1]. According to statistics, it is one of the most frequent accidents happening in industrial production and the transportation of hazardous materials [2]. The pool fire, representing a kind of diffusion flame driven by buoyancy forces [3, 4], is often used as a representative fire source to experimentally study the occurrence and development process of typical fire disasters. Besides,

pool fire itself also has a wide range of actual fire scenarios, such as fuel storage fire, fuel leakage fire, etc. Studying the occurrence and development of pool fire has a broad application background for fire accident prevention, fire detection, and performance-based fire protection design, etc.

Researches relevant to pool fires have been carried out for decades. Early and systematic experiments were conducted by Blinov and Khudyakov [4], who obtained the relationship between the fuel regression rate and pool diameter. Hottel [5] divided the combustion process into a laminar flow regime, a transition regime and a fully turbulent regime by Reynolds number, after analyzing Blinov and Khudyakov's data [4]. Afterward, the flame height [6-8], the plume temperature distribution [6, 9, 10], the flame pulsation frequency [11-14], the flame shape [15] and air entrainment [16] of pool fires were studied widely. However, almost all of the previous studies were based on none or small ullage height conditions, and the influence of ullage height on pool fire behaviors was ignored. While in reality, such as fuel storage fire, the ullage height will gradually increase as time goes by. And, during a fuel leakage accident, fuel may leak into a confining space, such as road sewer or ditch. In these conditions, ullage (storage ullage or the sewer sidewalls) above the fuel surface could directly influence the process of surrounding air entrained into the flame base, which further affects the initiation and upward development of plume entrainment vortexes and then influences the burning intensities. Besides, heat transfer from flame to the fuel through the ullage might also have an impact on the burning behaviors, depending on the fire size and the ullage thermal properties. Ullage height, as one of the major geometrical parameters of the system, can potentially alter the large-scale flow structures near the pool. This in turn can change the fire plume characteristics such as the flame height and its intermittency frequency, substantially. Therefore, analyzing its influence on flame characteristics would be crucial to make more scientific and targeted fire suppression and control strategies. However, to date, related studies are still very limited, only few literatures are available.

Magnus [17] investigated the combustion velocity and temperature distribution properties of gasoline and ethanol pool fires, and concluded that freeboard (pool ullage) concerned the amount of air entrained into the combustion zone. Artemenko and Blinov [18] experimentally studied the regression rate of pool fires involving aviation fuel and isoamyl alcohol, and found out that flame would self-extinguish as the ullage height is higher than a critical value. Dlugogorski and Wilson [19] studied the effect of vessel wall materials and ullage height on small-scale pool fires with diameters less than 70 mm, and found out that the mass loss rate decreases exponentially with the increase of ullage height within a certain range. Gao et al. [20] found out that the diesel and ethanol-diesel flame spread rate could be changed under different ullage height conditions. Kuang et al. [21] also analyzed the mass loss rate of pool fires under the effect of ullage height and crosswind, and found out that both have a significant effect on the mass loss rate.

In general, the above studies mainly discovered that ullage height can significantly affect the mass loss rate of pool fires. And a flame self-quenching phenomenon would happen when the ullage height increased to a critical value. However, the effect of ullage height on flame characteristics, such as flame height, oscillation properties, etc., were not studied. These flame characteristics directly determine the fire hazard and also are two key parameters to calculate the flame radiation to the surroundings.

Motivated by the above discussions, in the present study, experiments were conducted to investigate the evolution of flame characteristics of heptane and ethanol pool fires with diameters

of 10 cm, 15 cm, and 20 cm. For each pool, the ullage height was increased from zero to the value that the flame could not self-sustained. Physical interpretation of the effect of ullage height on pool fires was provided based on experimental observations and measurements. Following that, an equivalent hydraulic diameter, $D_{eq.}$, was proposed to quantitatively characterize the effect of ullage height on plume flow structures. New flame height and oscillation models were correlated based on the current study. The models were validated and agreed well with reference data collecting from 23 papers, which verified the reliability and universality of the new models.

2. Experimental Apparatus

A sketch diagram of the experimental setup used in this paper is demonstrated in Fig. 1. The inner diameter of the pools is 10 cm, 15 cm, and 20 cm. Fuel is supplied through the pool bottom, and the fuel level depth (ullage height) is maintained constant during each experimental condition. Different ullage heights are obtained by an electronic elevator through lifting or lowering the above fuel supply and level maintaining device. The maximum lifting range of the electronic elevator is 580 mm, and the adjusting accuracy is 1.5 ± 0.5 mm. An electronic balance with a maximum load of 34 kg and precision of 0.1 g, is used to record the fuel mass versus time with a sampling interval of 1 s. Several thermocouples are placed along the pool axis to record the centerline temperature profiles of the fire flume.

Digital Panasonic camera (HDC-TM700), with a spatial resolution of 1920 x 1080 and frame rates of 50 fps, is used to record the flame shape in front of the fuel pool. In table 1, the maximum flame height and the mean flame height were calculated from the pool upper rim to the flame tip where the flame intermittency respectively equals to 0.05 and 0.5 [16]. The detailed image processing method is as follows. As shown in Fig. 2, the first step is to convert the original image into a gray-scale image, then into a binary image, employing the Ostu method [22]. After that, the probability of the flame intermittency could be obtained as $p_i = n / N \quad (i = 1, 2, 3 \ldots)$, where n is the number of images that flame happens in the i - th pixel, N is the total number of the consecutive binary images. Finally, the colorized flame intermittency image could be plotted by Tecplot software, which gives the accurate pixel length of the maximum ($H_{f_{\max}}$) and average (H_f) flame height. Then, $H_{f_{\max}}$ and H_f are calculated by the pixel length multiplied by the calibrated length scale of each test. The reliability of this method has been proved by previous studies [23-25]. The maximum and average flame heights and the corresponding standard deviations are listed in table 1. Detailed experimental and model uncertainties are analyzed in appendix A.

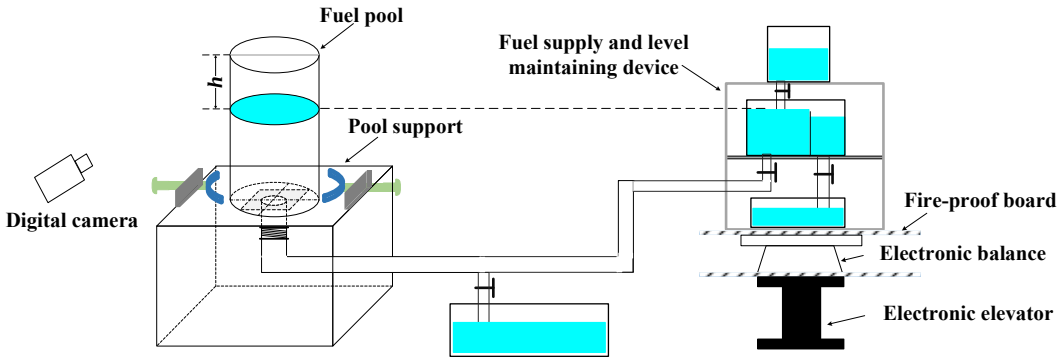

Fig. 1 Sketch diagram of the experimental setup.

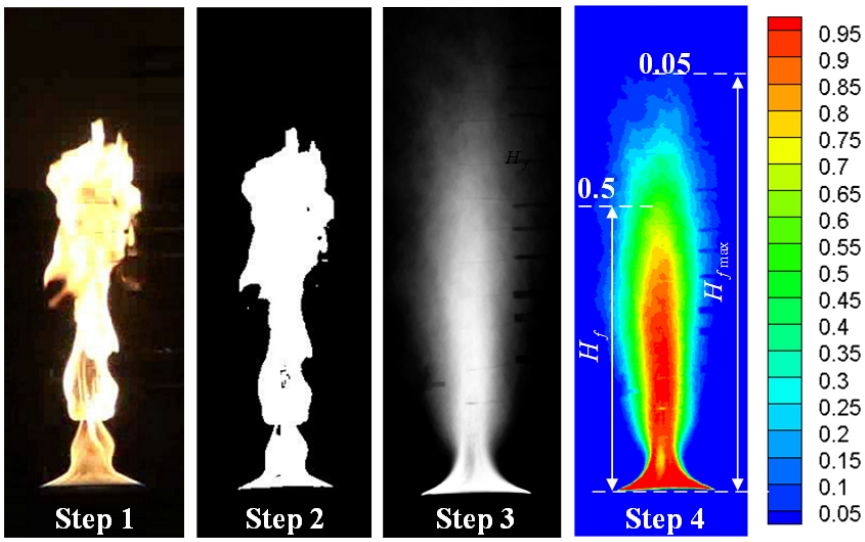

Fig. 2 Process of determining flame height.

Table 1 Experimental conditions and flame height.

Test Num.	D (cm)	h (mm)	h/D	Heptane			Ethanol		
				$H_{f_{\max}}$ (cm)	H_f (cm)	STD*	$H_{f_{\max}}$ (cm)	H_f (cm)	STD*
1	10	0	0	48.07	37.19	1.81	29.55	21.50	3.36
2		5	0.05	46.27	36.59	1.26	29.01	18.32	2.23
3		10	0.1	45.09	35.68	1.07	28.23	14.55	1.41
4		15	0.15	43.28	33.50	1.88	25.26	12.25	1.78
5		20	0.2	40.66	31.84	1.20	23.25	11.90	2.42
6		25	0.25	39.23	30.78	1.56	22.54	11.37	1.56
7		30	0.3	38.36	27.88	2.83	21.86	10.10	3.71
8		35	0.35	37.56	27.02	3.21	24.85	11.87	1.46

9		40	0.4	39.60	27.69	4.24	26.04	12.25	2.12
10		45	0.45	38.54	26.49	3.21	28.20	13.07	1.98
11		50	0.5	32.49	24.45	2.83	29.03	13.60	3.21
12		60	0.6	33.06	23.14	1.41	31.75	15.25	2.89
13		70	0.7	26.76	17.78	0.71	26.97	12.35	1.29
14		80	0.8	29.50	18.02	2.12	25.11	10.85	3.20
15		90	0.9	31.31	19.58	2.12	27.57	14.10	2.79
16		100	1	23.70	14.28	1.41	23.78	8.95	4.24
17		110	1.1	26.82	16.57	1.56	20.29	6.84	3.21
18		120	1.2	29.19	18.96	2.56	17.07	2.80	2.83
19		130	1.3	26.23	16.33	1.56	Self-extinction		
20		140	1.4	23.26	12.29	3.50			
21		150	1.5	Self-extinction					
22		0	0.00	73.95	58.97	4.21	47.85	32.46	3.28
23		7.5	0.05	71.27	55.37	4.70	40.24	25.80	3.27
24		15	0.10	69.01	51.37	4.46	37.74	23.84	3.35
25		22.5	0.15	66.05	46.22	4.32	32.47	19.97	3.51
26		30	0.20	60.55	42.43	4.10	29.68	17.30	3.46
27		37.5	0.25	61.96	41.56	4.12	27.61	15.26	3.28
28		45	0.30	55.61	40.25	4.87	29.48	15.43	3.34
29		52.5	0.35	58.29	37.82	4.38	25.53	12.74	3.26
30		60	0.40	54.34	35.85	4.29	22.74	11.12	3.37
31		67.5	0.45	48.55	31.97	4.99	22.42	11.61	3.82
32	15	75	0.50	43.05	27.85	3.29	32.27	16.41	4.39
33		90	0.60	44.17	26.86	4.93	28.64	13.68	4.54
34		105	0.70	42.48	25.83	4.49	32.47	14.79	4.10
35		120	0.80	42.90	27.71	6.63	28.84	9.01	5.04
36		135	0.90	44.46	28.65	5.65	29.39	10.24	4.07
37		150	1.00	42.48	28.60	5.50	12.08	3.57	5.39
38		165	1.10	44.88	30.16	6.35	22.89	6.37	4.60
39		180	1.20	42.81	27.47	5.93	Self-extinction		
40		195	1.30	33.73	19.10	6.21			
41		210	1.40	33.16	13.94	4.71			
42		225	1.50	Self-extinction					
43		0	0	100.28	77.50	5.47	55.30	37.50	4.36
44		20	0.1	91.62	72.69	3.54	54.01	35.09	1.41
45		40	0.2	90.16	67.48	2.78	48.34	30.02	3.20
46		60	0.3	85.04	63.09	1.41	46.53	28.13	2.70
47	20	80	0.4	79.55	57.88	3.71	53.07	31.48	1.41
48		100	0.5	74.43	53.77	3.20	52.90	32.00	1.41
49		120	0.6	66.02	45.99	2.70	53.84	34.15	1.41
50		140	0.7	67.03	44.81	3.60	53.24	32.86	0.71
51		160	0.8	74.71	49.10	1.31	47.74	27.52	3.07

52		180	0.9	74.89	51.02	1.41	49.11	29.24	1.41
53		200	1	75.16	51.48	2.41	46.19	28.21	4.70
54		240	1.2	66.66	40.51	4.24	40.51	21.42	4.80
55		280	1.4	59.16	32.55	6.09	29.07	12.39	1.70
56		320	1.6	56.97	36.30	2.12	25.54	9.55	5.66
57		360	1.8	42.70	20.39	3.54	Self-extinction		
58		400	2	36.85	15.91	5.45			
59		440	2.2	Self-extinction					

* STD: standard deviation

3. Results and Discussion

3.1 Flame characteristics

Based on experimental observation, as ullage height increases, the evolutions of flame characteristics with pool diameters of 10 cm, 15 cm, and 20 cm share a similar trend. Therefore, typical time-series snapshots (time interval, 0.08 s) of heptane and ethanol pool fires with D=15 cm under different non-dimensional ullage heights (h/D) conditions are shown in Fig. 3. As illustrated in Fig. 3, generally all snapshots show an unstable characteristic. In the viewpoint of fluid dynamics, the flame unstable characteristic results from the density differences between the rising fire plume gas and the surrounding cold air under the influence of gravity, which is called as Rayleigh-Taylor instability [26]. Besides, when h/D=0, it can be found from both heptane and ethanol flame snapshots that there is a relatively stable conical structure near the pool upper rim (below the red dash line), above which the unstable plume is developed.

This conical structure is formed due to the transverse pressure, induced by the horizontal component flow of the plume entrained airflow near the flame base. In this conical region, the slow combustion process (compared with the upper unstable region) mainly happens on the outer edge of the fire plume [27]. The overall density and velocity differences between this region and the surroundings are small. Then the influence of Rayleigh-Taylor instability is not predominant here. However, the heat released from this region will help to increase the density and velocity differences between upper plume and the surroundings, which then results in the development of an upper unstable plume.

As shown in Fig. 3, the flame characteristics are significantly changed with the increase of h/D.

Under lower ullage height conditions (typically, $0.1 \leq h/D \leq 0.5$ for heptane and $0.1 \leq h/D \leq 0.35$ for ethanol), the above mentioned conical structure disappears. And the unstable plume begins to initiate around the pool upper rim, then rolling and expanding upward. At the same time, its beneath flame is stretched thinner and thinner and eventually breaks from the bulk. This phenomenon is often called 'puffing' in literatures [13, 16]. The development of puffing will facilitate the mixing process of the fuel gas and the surrounding air, by entraining fuel gas from the plume to the surroundings and entraining nearby air into the plume. By comparing the puffing images of heptane or ethanol under different h/D conditions, it seems that the initiation and evolution of puffing are also influenced by h/D. However, as the h/D further increases, the puffing phenomenon becomes less evident. Through experimental observation, it could be found that more and more fuel gas was burnt within the pool. This means surrounding air is entrained into the pool, during which the formation of puffing might be disturbed and weakened.

According to Table 1, the maximum flame heights of heptane and ethanol show a decreasing trend as *h*/*D* increases. This could be explained as follows. The air entrainment restriction effect of pool ullage increases with *h*/*D*, resulting in a lower combustion intensity. Thus the fuel evaporation rate would be reduced due to the reduction of heat feedback to the fuel surface. Then the fuel gas would be burnt out at a shorter distance above the pool upper rim.

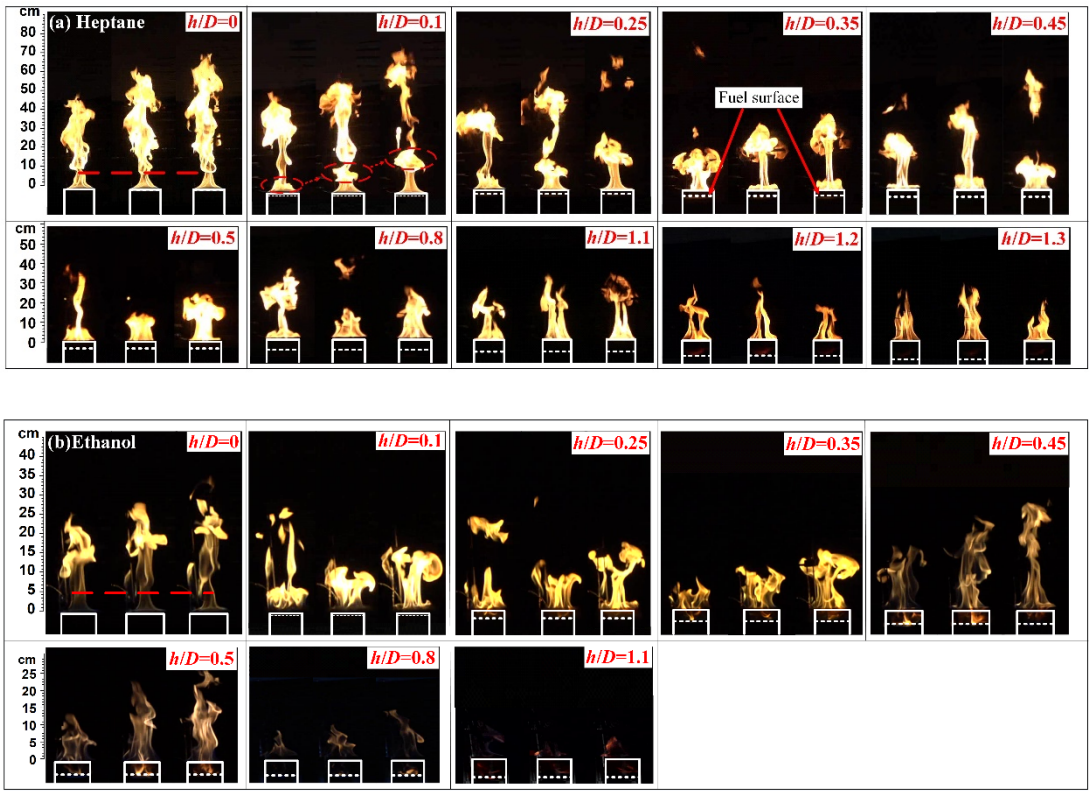

Fig. 3 Typical time-sequential experimental snapshots (*D*=15 cm) under different non-dimensional ullage height *h*/*D*: **(a)** heptane, **(b)** ethanol.

3.2 Mass loss rate

Figure 4 shows the typical fuel mass loss histories of repeated tests measured with different non-dimensional ullage height conditions (*h*/*D*=0, 0.2, 0.6, 1.1; *D*=15 cm). It can be observed that the current experimental results can be well repeated. According to Fig. 4, ullage height affects both the averaged mass rate of stable stage, and the mass loss rate profiles during the initial stage. Under lower ullage height conditions (*h*/*D*=0, 0.2), the profiles of the mass loss rate show a tendency to increase first and then stabilize. This could be explained that, when the pool ullage is small, fuel vapor will freely diffuse into the surroundings, resulting in lower fuel gas concentration above the fuel surface. When it is ignited, the initial burning rate is small. After that, heat feedback from the flame to the fuel surface leads to the increase of fuel surface temperature, and then a gradually increasing fuel evaporation rate (mass loss rate). The mass loss rate reaches a stable stage when the heat loss from the fuel surface gradually catches up with the received ones.

Under higher ullage height conditions (*h*/*D*=0.6, 1.1), the profiles of the mass loss rate rapidly increase to a peak value and then gradually decrease to the stable stage. The initial rapid increase

could be explained as follows. Before ignition, the initial fuel gas concentration near the fuel surface is high due to the confinement of pool ullage. Thus, at the beginning of the ignition, the combustion intensity is much higher than that of low ullage height conditions, so does the increase rate of mass loss rate profiles. After that, due to the confinement effect of pool ullage and the upward fuel gas evaporation movement, it is harder for the surrounding air entrained into the fuel surface, resulting in the flame base gradually detaching from the fuel surface and then the decrease of heat feedback received by the fuel surface. The mass loss rate decreases to the stable stage when the heat flux received by the fuel surface decreases to be equal to the heat loss.

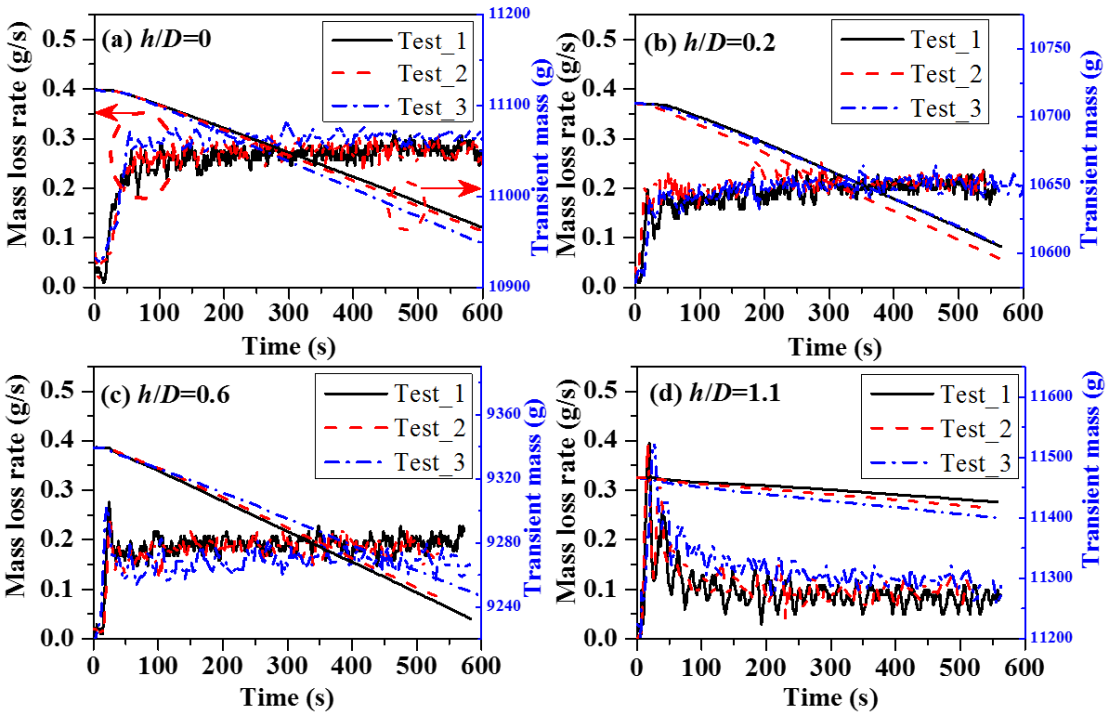

Fig. 4 Typical repeated experimental results for fuel mass loss history under different ullage height conditions with h/D=0, 0.2, 0.6, 1.1; D=15 cm.

The averaged mass loss rate against h/D of heptane and ethanol pool fires is plotted in Fig. 5. Generally, the profiles of the mass loss rate show a decreasing trend with the increase of h/D, resulting from the increased air entrainment restriction induced by the pool ullage. Besides, the mass loss rate of heptane decreases faster than that of ethanol, resulting in the mass loss rate of heptane being at first higher (h/D<0.5 for D=15 cm and 20 cm) and then lower ($h/D \geq 0.5$ for D=15 cm and 20 cm; $h/D \geq 0.4$ for D=10 cm) than that of ethanol. This trend could be explained that, compared with ethanol, per unit mass of heptane needs more oxygen for combustion. Then the increased air entrainment restriction effect would have a greater impact on heptane combustion processes. While for D=10 cm, when h/D<0.4 the mass loss rate differences minor between heptane and ethanol within experimental error.

In addition, as shown in Fig. 5, there is a stage (around $0.25 \leq h/D$<0.4 for heptane with D=10 cm, $0.25 \leq h/D$<0.35 for heptane with D=15 cm, and $0.7 \leq h/D$<1.0 for heptane with D=20 cm; $0.3 \leq h/D$<0.5 for ethanol with D=10 cm, 15 cm, and $0.4 \leq h/D$<0.8 for ethanol with D=20 cm) where

the mass loss rates of heptane and ethanol show an increasing trend. This might be relevant to the evolution of plume flow structures and the corresponding air entrainment with different *h*/*D* conditions. For example, as shown in Fig. 3(a) with *D*=15 cm, when *h*/*D*=0, the plumes of both heptane and ethanol show the highest turbulent intensity. Then, air entrainment, heat transfer to the fuel surface and mass loss rate would also be maximum in this case. When *h*/*D* increased to 0.1, their plume flow structures start to present a new pattern with the flame tip behaving like a coherent flow.

For heptane, the local peak mass loss rate (around *h*/*D*=0.4 for *D*=10 cm; *h*/*D*=0.35 for *D*=15 cm and *h*/*D*=1.0 for *D*=20 cm) might due to the full development of the 'coherent flow' structure, since the flame tip behaves very much like a counter flow non-premixed flame stabilization. Then strong entrainment and mixing processes are created near the plume tip, which feeds a relatively stable and turbulent non-premixed flame brush there.

While for ethanol, as shown in Fig. 3(b) with *D*=15 cm, as *h*/*D* increases to 0.35, this 'coherent flow' structure seems not to change much. With *h*/*D* further increases to 0.5, the plume shows a more turbulent characteristic. This might be caused by the increase of convective heat transfer between the flame base and the fuel surface, due to the thermal expansion effect induced by the inside combustion process as illustrated in Fig. 3(b). Then in this stage, the mass loss rate of ethanol shows a slightly increasing trend. Here, the plume flow evolution differences between heptane and ethanol might be the results of the following coupling effects: the heat transfer rate to the fuel surface, the fuel evaporation rate and the mixing process near the pool.

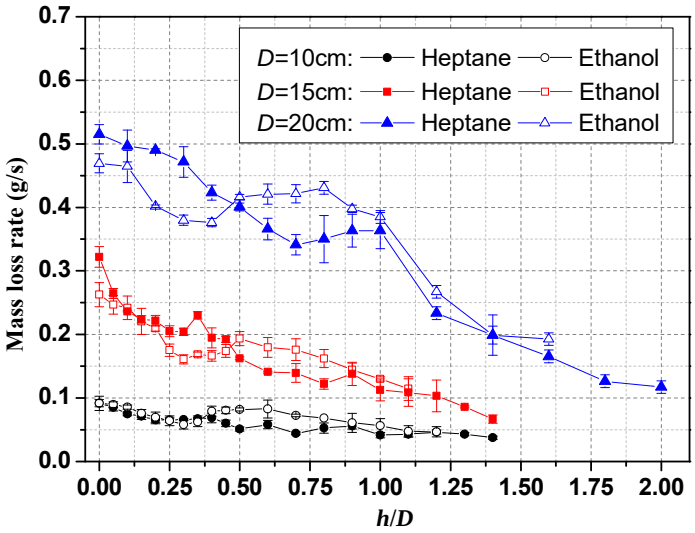

Fig. 5 Mass loss rate against non-dimensional ullage height, *h*/*D*.

3.3 Flame height

Heskestad [8] established the following classic model to calculate the buoyant diffusion controlled flame height, and the model has been verified by a variety of data from massive fire sources. The model is

$$H / D = 3.7Q^{*2/5} - 1.02 \qquad (1)$$

where *H* is the flame height, *D* is the diameter of fire source (or the effective diameter), Q^* is the

non-dimensional heat release rate, and is defined as

$$Q^* = Q / (\rho_o c_p T_o g^{\frac{1}{2}} D^{\frac{5}{2}}) \quad (2)$$

where Q is the dimensional heat release rate calculated by the mass loss rate. ρ_0 is the density of the ambient air, c_p is the specific heat of surrounding air, T_0 is the ambient temperature, g is the gravity acceleration.

Heskestad's model was obtained by data correction from experiments with none or rather small ullage height conditions. Dlugogorski and Wilson [19] conducted experiments with the non-dimensional ullage height ranging from 0 to 0.4, and found that Heskestad's model didn't work well under high ullage height conditions. Theoretically, Heskestad's model was developed by integrating the mass-entrainment rate of the fire plume from the fuel surface to the flame tip [8]. This works well with those unconfined conditions, whose entrainment process is only driven by the pressure differences within the flame horizontal and vertical directions. While for those under the effect of pool ullage, it is not the case. The existence of ullage height will affect the entrainment flow direction near the fuel surface and then the upward plume structures, as shown in Fig. 3.

Figure 6 shows the schematic of gas phrase flow with and without ullage height conditions. The fire plume not only flows upward but also has component motions which deviate from the upward flow at a certain angle due to the thermal expansion effect of fire plume. As shown in Fig. 6(a), when the ullage height equals to zero, this component motion will help to entrain more air into the plume. While under the confinement of pool ullage, the fire plume flow structure of both the base and upward are significantly changed. As shown in Fig. 6(b), the component motion of plume flow could be divided into *x* and *z* directions.

According to Newton's third law, that when two bodies act upon each other, the reaction force is always contrary and equal to the action force [28]. Thus, when the plume flow flows to the pool ullage from *x* and *z* directions, as shown in Fig. 6, the reaction force from the pool ullage to the plume flow could then be divided into x_c and z_c directions. Then, according to the definition of hydraulic diameter, the force balance for fire plume within the pool could be given,

$$\bar{P}\int dA = \bar{\tau}\int dC \int dw \quad (3.1)$$

where $\bar{P}$ is the area-averaged plume pressure driven by the thermal expansion effect, *dA* is the interface area between the plume flow and the pool ullage. In the current study, $\int dA = S_{lip} + S_{pool}$, where S_{lip} and S_{pool} are the areas of the pool ullage and the burning surface. In the current study, all tests are conducted in still air. And, the plume flow is symmetric around the center axis of the pool. Then, the shear force would also be symmetrically around the pool center axis when the plume flow is fully developed. It is reasonable to use $\bar{\tau}$ to donate the linear-averaged shear force around the circumference. *dC* is the contact perimeter between plume flow and the pool, $\int dC = \pi D$. *dw* is the width of the analyzed control volume.

While for an equivalent circular case, it can be expressed as follows,

$$\bar{P}\pi D_{eq.}^2 / 4 = \bar{\tau}\pi D_{eq.}\int dw \tag{3.2}$$

where $D_{eq.}$ is the equivalent hydraulic diameter. By combining Eq. (3.1) & (3.2), it can be given as,

$$D_{eq.} = \frac{4\int dA}{\int dC} \tag{4}$$

where currently Eq. (4) can be further simplified as $D_{eq.} = 4(S_{lip} + S_{pool})/\pi D = D + 4h$.

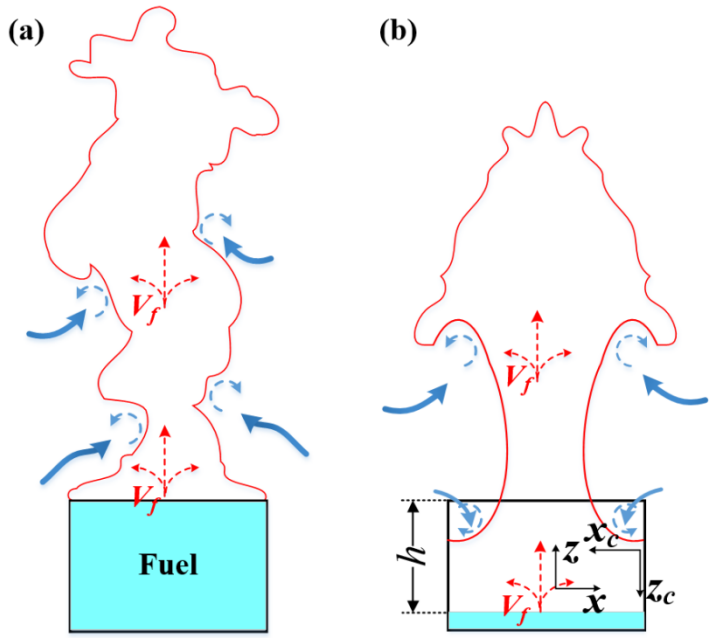

Fig. 6 The schematic of gas phrase flow, (a) without ullage (b) with ullage.

According to Eq. 4, when S_{lip} = 0 (or ullage height h=0), $D_{eq.} = D$. This means that the proposed equivalent hydraulic diameter covers the zero ullage height conditions. Based on Heskestad's study, we can obtain a modified non-dimensional heat release rate, Q_{lip}^* by substituting Eq. (4) into Eq. (2), $Q_{lip}^* = Q/(\rho_0 c_p T_0 g^{1/2}(D_{eq.})^{5/2})$. The modified non-dimensional flame length is defined as $H_f / D_{eq.}$. Concerning previous studies [29, 30], $H_f / D_{eq.}$ is the function of Q_{lip}^* and can be represented as $H_f / D_{eq.} = fcn(Q_{lip}^*)$. The relationship of $H_f / D_{eq.}$ against Q_{lip}^* was plotted in Fig. 7, and also compared with reference data [31-33] with h/D ranging from 0.01 to 0.53. Figure 7 shows that the proposed equivalent hydraulic diameter $D_{eq.}$ works well with pool fires under the effect of ullage height, and the correlated

models are summarized as follows.

$$\frac{H_f}{D_{eq.}} = \begin{cases} 3.48 Q_{lip}^{*\ 0.43} - 0.11 \text{ , for Heptane} \\ 2.34 Q_{lip}^{*\ 0.67} + 0.10 \text{ , for Ethanol} \end{cases} \quad (5)$$

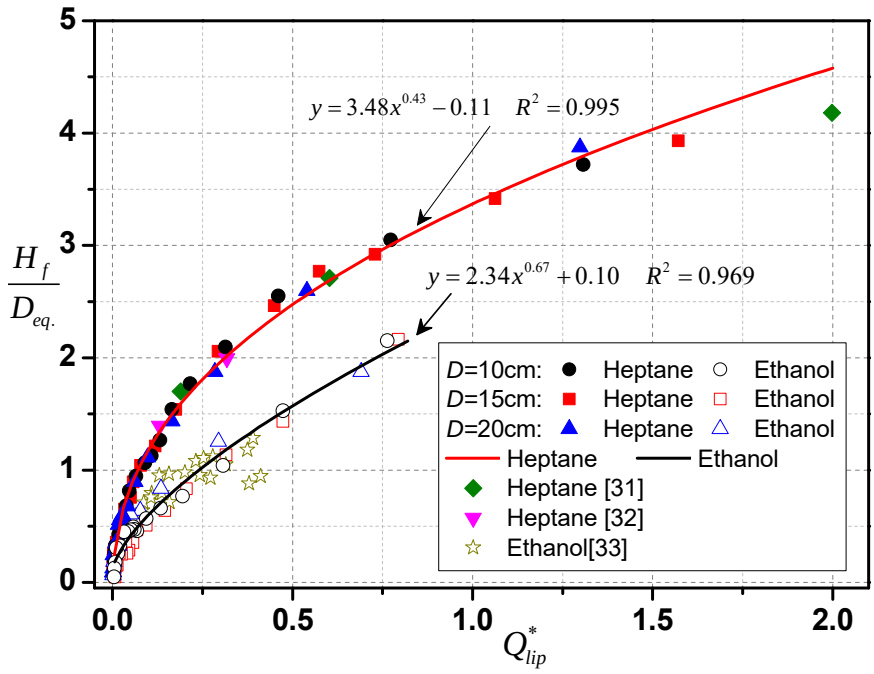

Fig. 7 Normalized flame height $H_f / D_{eq.}$ against modified normalized HRR Q_{lip}^*.

3.4 Flame oscillation frequency

In the current study, the flame oscillation frequency is calculated by time-series flame height data after Fast Fourier Transform (FFT). This method has been successfully used in previous works [34-36]. Figure 8(a) shows the time-series flame height data of 40 s (2000 frames) of the steady combustion stage, obtained by the image processing method (detailed descriptions are given in Section 2). The corresponding spectrum curve is depicted in Fig. 8(b), from which the main flame oscillation frequency could be easily obtained.

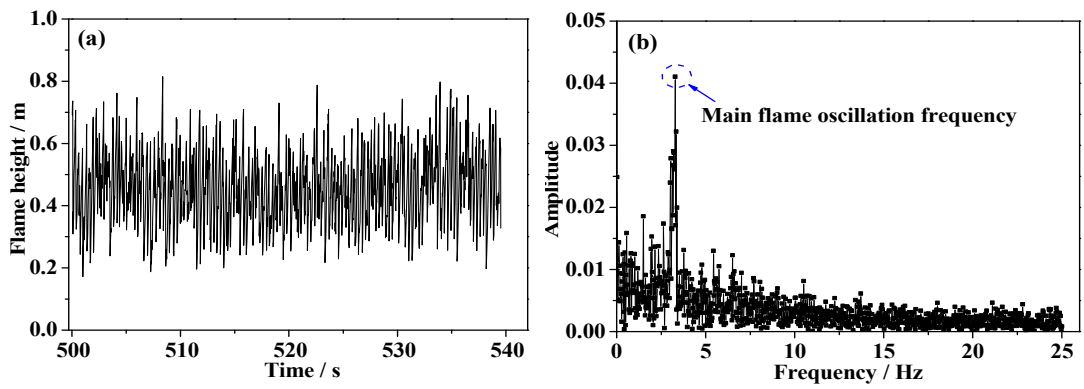

Fig. 8. Time-series flame height **(a)** and amplitude spectrum **(b).**

3.4.1 Comparison with previous dimensional models

Previous studies have been investigating the flame oscillation frequency for decades, and many empirical models were established with similar forms as $f \propto 1/\sqrt{D}$. Pagni [11] fitted an equation between flame oscillation frequency and the pool diameter (or equivalent diameter) as $f = \sqrt{2.3/D}$, based on massive experimental data obtained from plenty of fuels. Bejan [12] reanalyzed Pagni's model based on the buckling theory of inviscid streams and gave it as $f = \sqrt{3.1/D}$ (for round plume) and $f = \sqrt{2.7/D}$ (for two-dimensional plume). Malalasekera et al. [13] fitted it as $f = \sqrt{2.82/D}$, with burner diameters ranging from 0.0074 m to 2.2 m. It should be noted that the above dimensional flame oscillation models didn't consider the effect of ullage height, thus it maybe not applicable to pool fires under the effect of ullage height.

Figure 9 demonstrates the flame oscillation frequency in all cases in this work. As shown in Fig. 9, generally the flame oscillation frequency of heptane and ethanol pool fires tend to decrease with the increase of *h*/*D*. This trend could be explained that the initiation and formation of the vertical toroidal structure at the flame base are significantly influenced by the pool ullage height, due to its inhibition effect on the surrounding air flowing to the flame base to form the upward entrainment vortexes. Model predictions of Pagni [11], Bejan [12] and Malalaskera et al. [13] are also shown in Fig. 9, which shows that these models are only applicable to pool fires with minor ullage height (*h*/*D*) conditions. The errors of these model predictions increase with the increase of *h*/*D*.

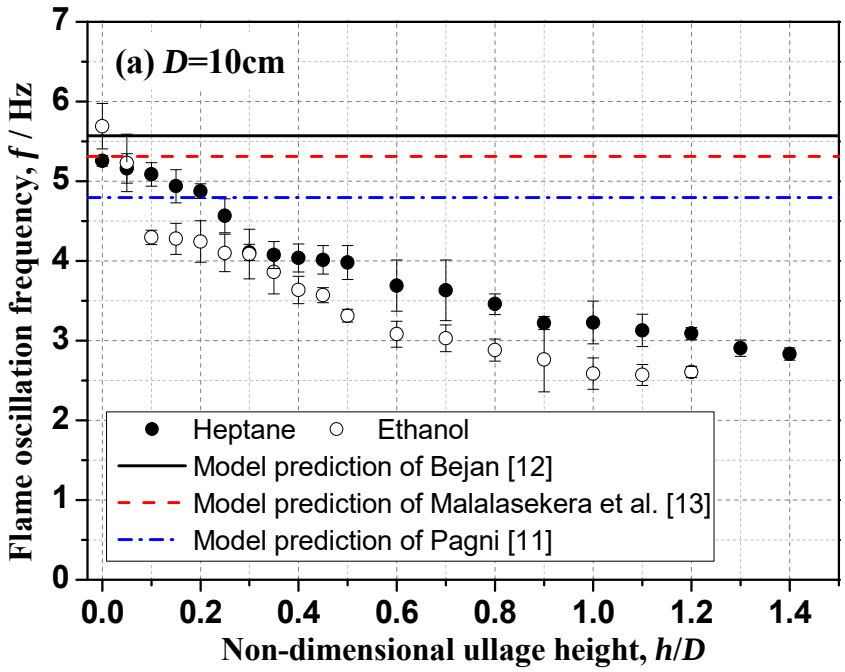

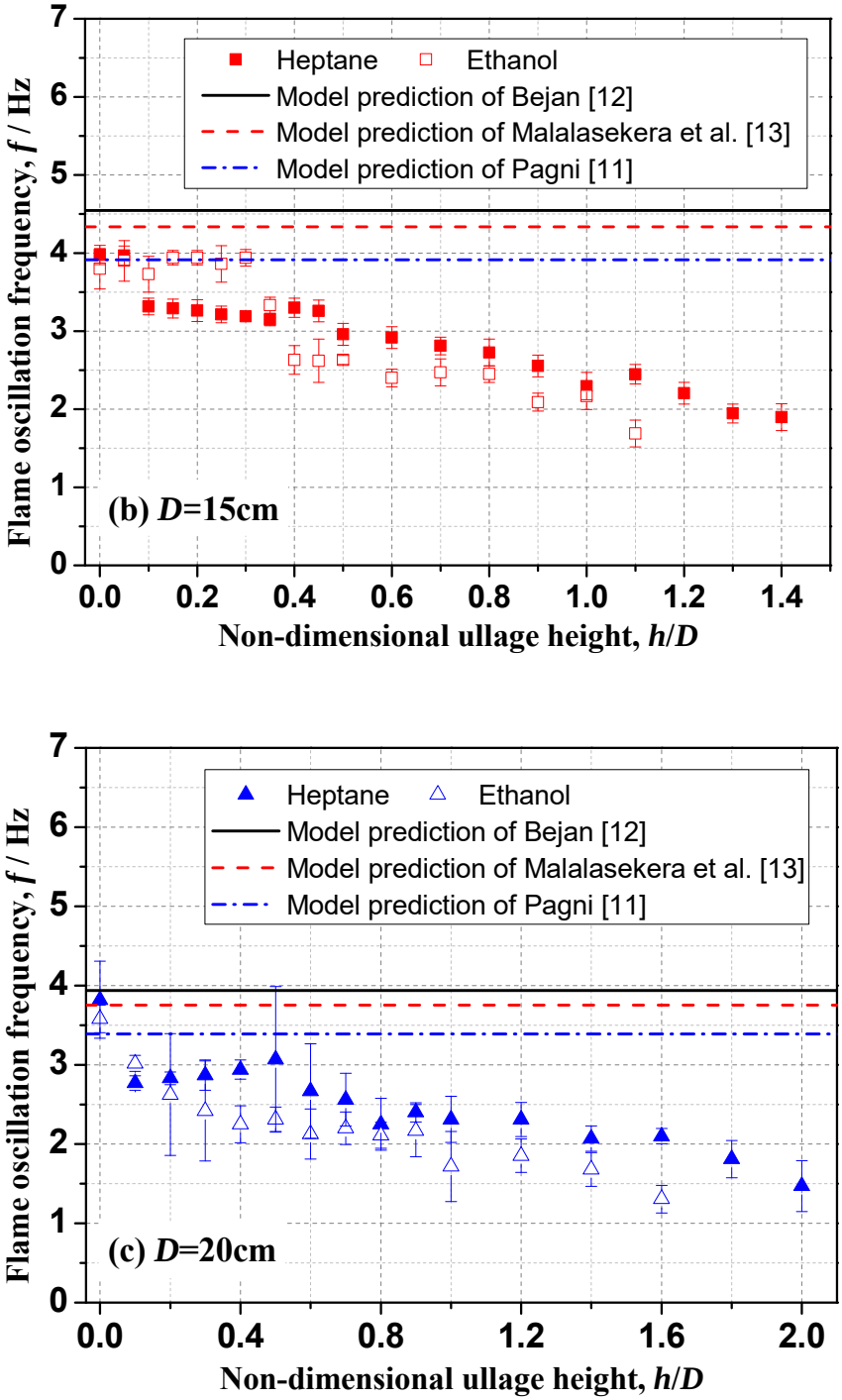

Fig. 9. Comparisons with previous dimensional models, (a) D = 10 cm, (b) D = 15 cm, (c) D = 20 cm.

3.4.2 Comparison with previous dimensionless models

By dimensionless analysis, Emori and Saito [37] emphasized the importance of the Stouhal (St) and Froude (Fr) numbers, which were defined as

$$St = \frac{fL}{V_f} \tag{6}$$

$$Fr = \frac{V_f^2}{Lg} \tag{7}$$

where L is the characteristic length, and it is the pool diameter (L=D) for circular pool fires. g is the gravitational acceleration. V_f is the characteristic velocity, which refers to the evaporation velocity of liquid pool fires, and is calculated through the theory of ideal gas law,

$$PV = nRT \tag{8}$$

$$n = \frac{m'}{M} \tag{9}$$

$$V_f = \frac{V}{A} \tag{10}$$

where R is the ideal gas constant, m' is the mass loss rate, M is the molar mass, n is the number of moles of gas, A is the burning area. P, V and T are the pressure, volume and absolute temperature, respectively. Substituting Eq. (8) & (9) into Eq. (10), one can obtain,

$$V_f = \frac{m'RT}{MPA} \tag{11}$$

substitute Eq. (11) into Eq. (6) & (7), one can obtain St and Fr. Malalasekera et al. [13] given the best-fit approximation of St vs. $1/Fr$ as $St = 0.52(1/Fr)^{0.505}$. Sato et al. [38] fitted it as $St = 0.517(1/Fr)^{0.502}$.

Figure 10 shows the comparisons of the current experimental data with previous dimensionless models. According to Fig. 10, the prediction models from Malalaskera et al. [13] and Sato et al. [38] generally work well with small ullage height conditions. Similar to the above dimensional models, the error between model predictions and experimental results increases with the increase of ullage height.

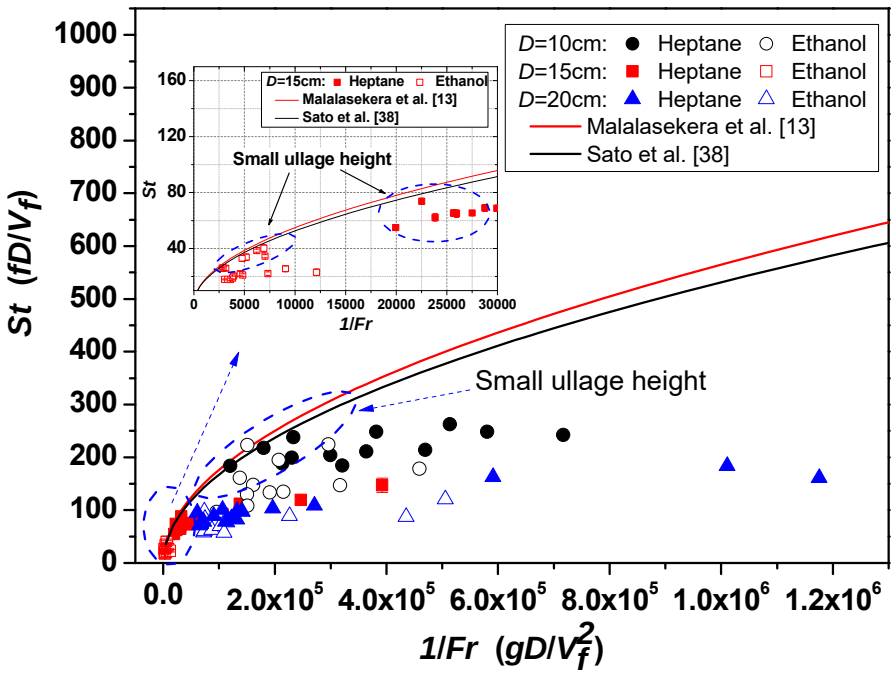

Fig. 10. Comparisons with previous dimensionless models.

3.4.3 New flame oscillation models

As discussed in section 3.3, here the equivalent hydraulic diameter $D_{eq.}$ was employed to take the effect of ullage height on flame oscillation behaviors into account. As for the dimensional model, according to the buckling theory of inviscid streams [12, 38], there exists a functional relationship between f and -0.5 power of D. Thus, new correlations were correlated by fitting f against $D_{eq.}^{-0.5}$, which yields $f = 1.8\ D_{eq.}^{-0.5}$. To validate this new correlation, as demonstrated in Fig. 11, previous experimental data collecting from thirteen papers [37, 39-50] were employed, and they agreed well with the new correlation.

Substituting Eq. (4) into Eq. (6) and (7), one can obtain the modified St^* and Fr^*, which were plotted in Fig. 12. A new dimensionless model, $St^* = 0.49(1/Fr^*)^{0.52}$, was obtained based on the current experimental data. Seven reference papers [13, 14, 16, 36, 39, 41, 45] were used here for validation, which showed that the new dimensionless model also has good universality. In summary, dimensional and dimensionless flame oscillation models are summarized as follows.

Dimensional flame oscillation model:

$$f = 1.8 D_{eq.}^{-0.5} \tag{12a}$$

Dimensionless flame oscillation model:

$$St^* = 0.49(1/Fr^*)^{0.52} \tag{12b}$$

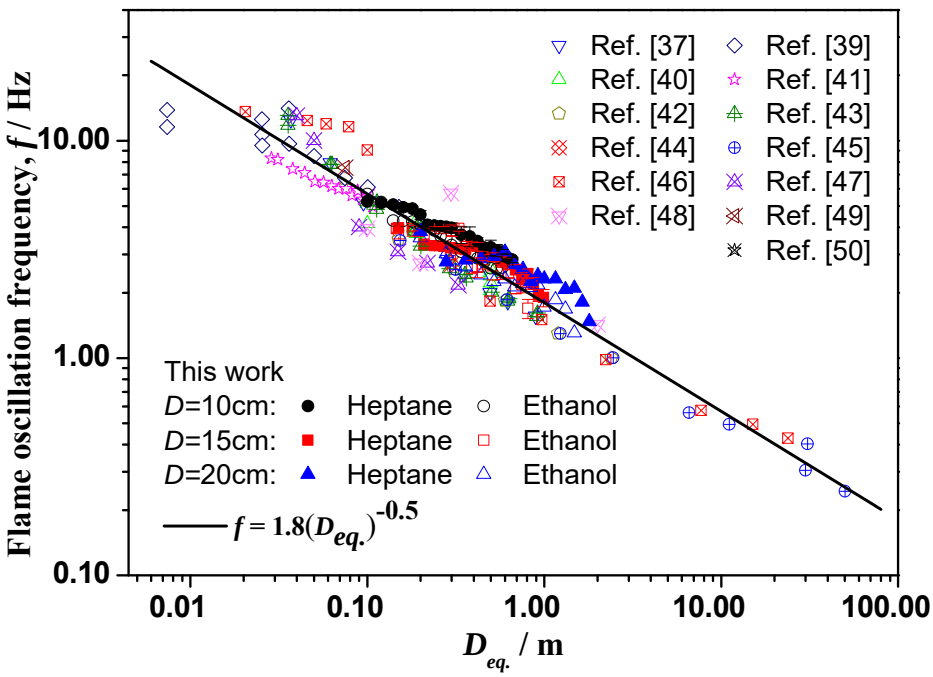

Fig. 11. New dimensional flame oscillation model.

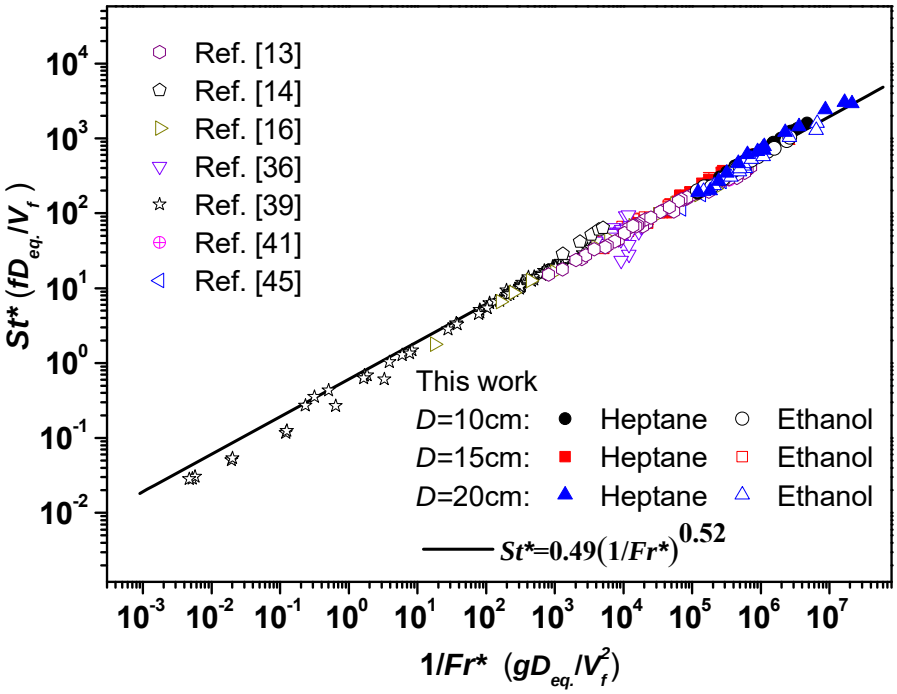

Fig. 12. New dimensionless flame oscillation model.

4. Conclusions

In this work, a series of experiments were performed to study the effect of ullage height on flame characteristics of heptane and ethanol pool fires. Based on experimental observation and measured data, the influencing mechanism of ullage height is systematically interpreted. The work and major conclusions are summarized as follows.

(1) Ullage height has a significant effect on flame characteristics. When the ullage height equals zero, a stable conical plume structure is maintained near the pool upper rim, above which the unstable plume develops. Under lower ullage height conditions, plume puffing happens. The unstable plume begins to initiate around the pool upper rim, then rolling and expanding upward. Meanwhile, its beneath flame is stretched thinner and thinner and eventually breaks from the bulk. As the ullage height further increases, puffing becomes less evident. While for the mass loss rate, it generally decreases with the increase of ullage height, due to the increased air entrainment restriction induced by the pool ullage. Besides, the mass loss rate of heptane decreases faster than that of ethanol.

(2) To consider the effect of ullage height on plume flow structures, an equivalent hydraulic diameter $D_{eq.}$ was proposed to modify the previous flame height model. The established new flame height models were validated and agreed well with the reference data.

(3) By comparing previous model predictions with the current experimental data, this study proves that conventional dimensional and dimensionless flame oscillation models are unsuitable to pool fires with large ullage height. Based on $D_{eq.}$, new flame oscillation models are correlated. The reliability and universality of the new correlations are validated by reference data.

The findings in this study have the following potential applications. The new flame height model (Eq. (5)) considering the effect of ullage height could be used to further calculate the

radiative heat flux of pool fires to the surroundings [51]. Then, fire safety distance between fuel storage tanks and its nearby facilities could be obtained. Fuel thickness sensors in the fuel container might be destroyed by fire accidents, and Eq. (12a) proposes an easy-to-implement way to deduce it. Future work is essential to investigate the influences of ullage height on flame behaviors and the heat transfer mechanisms inside the pool.

Acknowledgement

This work was supported by the National Natural Science Foundation of China (NSFC) under Grant No. 51722605, the Fundamental Research Funds for the Central Universities under Grant No. WK2320000038 and WK2320000042, and the National Post-doctoral Program for Innovative Talents (Grant No. BX20180288).

Appendix A. Uncertainty analysis

Due to the unavoidable measurement error and accumulated error in the process of model deduction, it is essential to quantitatively estimate their impact on the results' uncertainty. In this study, uncertainty analysis is conducted according to previous studies [52, 53]. The measuring devices used during the experiment include an electronic balance and an HD camera to record the transient fuel mass and flame shape, with sampling intervals of 1 s and 0.02 s respectively. These sampling intervals are much higher than the output time length of experiments (also called as "autocorrelation time" [53]), which means that the current study belongs to single sample tests [52]. In single-sample uncertainty analysis, the model uncertainty is described by a root-sum-square (RSS) equation [52, 53],

$$\delta R = \left\{ (\frac{\partial R}{\partial x_1}\delta x_1)^2 + (\frac{\partial R}{\partial x_2}\delta x_2)^2 + ... + (\frac{\partial R}{\partial x_N}\delta x_N)^2 \right\}^{1/2} \tag{A1}$$

where $x_i (i = 1,2,3,...,N)$ is the measurement, R is the experimental result which is calculated from a set of measurements, $R = (x_1, x_2, x_3, ..., x_N)$. The partial derivative of R concerning x_i, $\frac{\partial R}{\partial x_i}$, is the sensitivity coefficient representing the influence weight of x_i on R. $\delta x_i (i = 1,2,3,...,N)$ is the uncertainty of x_i, in the single-sample analysis it represents 2σ, where σ is the standard deviation of x_i. A more commonly used way to describe the uncertainty is by a fraction, such as relative uncertainty, rather than in engineering units as shown in Eq. (A1). Besides, the result R could generally be expressed as a product string with the dominated uncertain terms taken into account as $R = (x_1^a x_2^b x_3^c, ..., x_M^m)$. Then the relative uncertainty of R could be expressed as [52, 53],

$$\frac{\delta R}{R} = \left\{ (a\frac{\delta x_1}{x_1})^2 + (b\frac{\delta x_2}{x_2})^2 + ... + (m\frac{\delta x_M}{x_M})^2 \right\}^{1/2} \tag{A2}$$

The uncertainties of the measurements and deduced models are listed in Table A1. In the table, the uncertainties of the first four parameters including ullage height (h) controlled by the fuel supply devices, mass loss rate (m') derived from the electronic balance recording, flame height (H_f) processed from video recording and flame oscillation frequency (f) calculated by time-series flame height data after Fast Fourier Transform (FFT) is determined based on the experimental results. The uncertainties of the deduced models are calculated based on the uncertainty sources. For example, Eq. (12b) could be rewritten as $V_f^{2b-1} D_{eq.}^{1-b} f = g^b a$ according to Eqs. (6) ~ (11), where a=0.49, b=0.52. Based on Eq. (A2), the model uncertainty could be determined as $\left\{\left[(2b-1)\frac{\delta V_f}{V_f}\right]^2+\left[(1-b)\frac{\delta D_{eq.}}{D_{eq.}}\right]^2+(\frac{\delta f}{f})^2\right\}^{1/2} = \left[(0.04\times 7.04)^2+(0.48\times 2.2)^2+7.16^2\right]^{1/2} = 7.24\%$.

Table A1 Measurement and model uncertainties

Parameters	Uncertainty sources	Relative uncertainty, %	Final relative uncertainty, %
h	Exp.	± 2.2	± 2.2
m'	Exp.	± 7.04	± 7.04
H_f	Exp.	± 18.22	± 18.22
f	Exp.	± 7.16	± 7.16
Eq. (4)	h	± 2.2	± 2.2
Eq. (5)	H_f	± 18.2	± 8.92
	m'	± 7.04	
	h	± 2.2	
Eq. (11)	m'	± 7.04	± 7.04
Eq. (12a)	f	± 7.16	± 7.24
	h	± 2.2	
Eq. (12b)	V_f (or m')	± 7.04	± 7.24
	f	± 7.16	
	h	± 2.2	

References

1. W. C. Fan, Q. G. Wang, F. H. Jiang, A Brief Course of Fire Science. Anhui Hefei: Press of University of Science and Technology of China, 1995

2. Planas-Cuchi, E., H. Montiel, and J. Casal, A survey of the origin, type and consequences of fire accidents in process plants and in the transportation of hazardous materials. Process Safety and Environmental Protection, 75(1997) 3-8.

3. Nakakuki, A., Liquid fuel fires in the laminar flame region. Combustion and flame, 23(1974) 337-346.

4. Blinov, V. and G. Khudyakov, Diffusion burning of liquids, Army Engineer Research and Development Labs Fort Belvoir VA, 1961.

5. Hottel, H. Certain laws governing the diffusive burning of liquids by Blinov and Khudiakov (1957). in Fire Research Abstracts and Reviews. 1959.

6. McCaffrey, B., Purely buoyant diffusion flames: Some experimental results. Final Report. Chemical and Physical Processes in Combustion. The National Institute of Standards and Technology (NIST), Miami Beach, 1979

7. Becker, H. and D. Liang, Visible length of vertical free turbulent diffusion flames. Combustion and Flame, 32(1978) 115-137.

8. Heskestad, G., Fire plumes, flame height, and air entrainment, in SFPE handbook of fire protection engineering, Springer, 2016.

9. Beyler, C.L., Fire plumes and ceiling jets. Fire safety journal, 11(1986) 53-75.

10. J. Ji, C. Fan, W. Zhong, X. Shen, J. Sun, Experimental investigation on influence of different transverse fire locations on maximum smoke temperature under the tunnel ceiling, International Journal of Heat and Mass Transfer 55 (2012) 4817-4826.

11. Pagni, P., Pool fire vortex shedding frequencies. Appl. Mech. Rev, 43(1990) 160.

12. Bejan, A., Predicting the pool fire vortex shedding frequency. Journal of Heat Transfer, 1991.

13. Malalasekera, W., H.K. Versteeg, and K. Gilchrist, A review of research and an experimental study on the pulsation of buoyant diffusion flames and pool fires. Fire and materials, 20(1996) 261-271.

14. Tang F., Hu L., Wang Q. and Ding Z., Flame pulsation frequency of conduction-controlled rectangular hydrocarbon pool fires of different aspect ratios in a sub-atmospheric pressure. International Journal of Heat and Mass Transfer, 76(2014) 447-451.

15. Cetegen, B. and Y. Dong, Experiments on the instability modes of buoyant diffusion flames and effects of ambient atmosphere on the instabilities. Experiments in Fluids, 28(2000) 546-558.

16. Zukoski, E.E., T. Kubota, and B. Cetegen, Entrainment in fire plumes. Fire safety journal, 3(1981) 107-121.

17. Magnus, G. Tests on combustion velocity of liquid fuels and temperature distribution in flames and beneath surface of the burning liquid. in Proc. 1st Int. Symp. on the Use of Models in Fire Research. 1961.

18. Artemenko, E. and V. Blinov, Burning of liquids in vessels with change of level. Combustion, Explosion and Shock Waves, 4(1968) 39-42.

19. Dlugogorski, B. and M. Wilson, Effect of Ullage on Properties of Small-Scale Pool Fires. Developments in Chemical Engineering and Mineral Processing, 8(2000) 149-166.

20. Z. Gao, S. Lin, J. Ji, M. Li, An experimental study on combustion performance and flame spread characteristics over liquid diesel and ethanol-diesel blended fuel, Energy 170 (2019) 349-355.

21. Kuang C., Hu L., Zhang X., Lin Y. and Kostiuk L. An experimental study on the burning rates of n-heptane pool fires with various lip heights in cross flow. Combustion and Flame 201 (2019) 93-103.

22. Otsu, N., A threshold selection method from gray-level histograms. IEEE transactions on systems, man, and cybernetics, 9(1979) 62-66.

23. Liu C, Wan H, Ji J. et al. Flame spread characteristics and a multi-cylinder radiation model for diesel tray fires against a sidewall. International Journal of Thermal Sciences. 139(2019) 433-439.23.

24. Tang, F., Q. He, and J. Wen, Effects of crosswind and burner aspect ratio on flame characteristics and flame base drag length of diffusion flames. Combustion and Flame, 200(2019) 265-275.

25. Gao Z., Ji J., Wan H. et al., An investigation of the detailed flame shape and flame length under the ceiling of a channel. Proceedings of the Combustion Institute, 35(2015) 2657-2664.
26. De Ris, J. and L. Orloff, A dimensionless correlation of pool burning data. Combustion and Flame, 18(1972) 381-388.
27. Ghoniem, A.F., I. Lakkis, and M. Soteriou. Numerical simulation of the dynamics of large fire plumes and the phenomenon of puffing. in Symposium (International) on Combustion. Elsevier, 26(1996):1531-1539.
28. Knight, R.D., Physics for scientists and engineers. 2017: Pearson Higher Ed.
29. Hasemi Y., Tokunaga T., Some Experimental Aspects of Turbulent Diffusion Flames and Buoyant Plumes from Fire Sources Against a Wall and in a Corner of Walls, Combustion Science and Technology, 40 (1984) 1-18.
30. Heskestad, G. Peak gas velocities and flame heights of buoyancy-controlled turbulent diffusion flames. in Symposium (International) on Combustion, Elsevier 1981.
31. Hamins, A., et al., Estimate of flame radiance via a single location measurement in liquid pool fires. Combustion and flame, 86(1991) 223-228.
32. Kang Quansheng, Study on Burning Characteristic and Heat Feedback of Unsteady Combustion Process of Small Scale Pool Fires. Hefei: University of Science and Technology of China, 2009.
33. Tao Changfa, The study of Combustion Characteristic and Heat Transfer Meehanism of Alcohol Pool Fire under Oblique Air Flow. Hefei: University of Science and Technology of China, 2013
34. Cetegen, B.M. and T.A. Ahmed, Experiments on the periodic instability of buoyant plumes and pool fires. Combustion and Flame, 93(1993) 157-184.
35. Chen X., Lu S. and Wang X. et al., Pulsation behavior of pool fires in a confined compartment with a horizontal opening. Fire technology, 52(2016) 515-531.
36. Fang J., Tu R. and Guan J. et al., Influence of low air pressure on combustion characteristics and flame pulsation frequency of pool fires. Fuel, 90(2011) 2760-2766.
37. Emori, R.I. and K. Saito, A Study of Scaling Laws in Pool and Crib Fires. Combustion Science and Technology, 31(1983) 217-231.
38. Sato, H., K. Amagai, and M. Arai, Scale modeling of puffing frequencies in pool fires related with Froude number, in Progress in Scale Modeling. Springer, (2008) 133-147.
39. Hamins, A., J. Yang, and T. Kashiwagi. An experimental investigation of the pulsation frequency of flames. in Symposium (International) on Combustion, Elsevier, 1992.
40. Zukoski, E., B. Cetegen, and T. Kubota. Visible structure of buoyant diffusion flames. in Symposium (International) on Combustion, Elsevier, 1985.
41. Sibulkin, M. and A.G. Hansen, Experimental study of flame spreading over a horizontal fuel surface. Combustion Science and Technology, 10(1975) 85-92.
42. Byram, G.M. and R.M. Nelson, The modeling of pulsating fires. Fire Technology, 6(1970) 102-110.
43. Portscht, R., Studies on characteristic fluctuations of the flame radiation emitted by fires. Combustion Science and Technology, 10(1975) 73-84.
44. Weckman, E. and A. Sobiesiak. The oscillatory behaviour of medium-scale pool fires. in Symposium (International) on Combustion, Elsevier, 1989.
45. Baum, H.R. and B. McCaffrey, Fire induced flow field-theory and experiment. Fire Safety

Science, 2(1989) 129-148.
46. Schönbucher, A., Arnold B. and Banhardt V. et al. Simultaneous observation of organized density structures and the visible field in pool fires. in Symposium (International) on Combustion, Elsevier, 1988.
47. Hertzberg, J., M. Namazian, and L. Talbot, A laser tomographic study of a laminar flame in a Karman vortex street. Combustion Science and Technology, 38(1984) 205-216.
48. Brötz W., Schönbucher A., Scheller, V. et al., Electronically produced equidensities from time exposures and instantaneous photographs in the investigation of pool flames. Combustion and Flame, 37(1980) 1-24.
49. Walton S., He X. and Zigler, BT et al., An experimental investigation of the ignition properties of hydrogen and carbon monoxide mixtures for syngas turbine applications. Proceedings of the Combustion Institute, 31(2007) 3147-3154.
50. Hagglund, B. and L. Persson, An experimental study of the radiation from wood flames. Forvarets Forhningsanstalt, FAO, 1974.
51. H. Wan, Z. Gao, J. Ji, J. Sun, Y. Zhang, K. Li, Predicting heat fluxes received by horizontal targets from two buoyant turbulent diffusion flames of propane burning in still air, Combustion and Flame 190 (2018) 260-269.
52. Moffat, Robert J. Using uncertainty analysis in the planning of an experiment. Journal of Fluids Engineering 107(1985) 173-178.
53. Moffat, Robert J., Describing the uncertainties in experimental results. Experimental thermal and fluid science 1(1988) 3-17.